

First-principles LCPAO Approach to Insulators Under Finite Electric Fields

Naoya Yamaguchi^{a,*}, Fumiyuki Ishii^{a,**}

^a*Nanomaterials Research Institute (NanoMaRi), Kanazawa University*

Abstract

We developed the linear-combination-of-pseudo-atomic-orbitals (LCPAO) scheme of a finite electric field method based on the modern theory of polarization. Our implementation successfully evaluated the dielectric constants and Born effective charges of typical semiconducting and insulating materials. Our formalism will become a powerful tool to expand subjects of researches on materials under electric fields.

Keywords: electric field; density functional theory; LCAO; Berry phase; dielectric constant; first-principles calculation.

1. Introduction

Electric field effects on insulators have been getting much attention and investigated both experimentally and theoretically owing to scientific interest as well as applications. In theoretical works based on quantum mechanics, dielectric properties including responses for electric fields have intensively investigated for more than a half century [1–3]. After the modern theory of polarization (MTP) was derived [4], first-principles calculations of insulating solids are capable of determining values of electric polarization as well-defined bulk quantities with Berry phases. In addition, polarization and Berry phases allow us to describe electronic structures of solids under electric fields [5].

The MTP solved a difficulty in describing electric polarization in bulk insulators with Berry phases obtained from overlap matrices between the periodic parts of Bloch orbitals at a k-point and the next k-point instead

**E-mail address:* n-yamaguchi@cphys.s.kanazawa-u.ac.jp

***E-mail address:* ishii@cphys.s.kanazawa-u.ac.jp

of explicit evaluation of the position operator. The difficulty comes from the periodic boundary condition applied in electronic structure calculations based on the density functional theory (DFT), and one cannot find how electrons cross the cell boundary because existence of electrons is described by continuous electronic densities. In introducing electric fields into DFT frameworks, the boundary makes another difficulty that the periodicity can give unphysical fields. Additional potential for finite electric fields includes the term of the product of an electric field and the position operator $\mathbf{E} \cdot \mathbf{r}$, but it is not acceptable when there are electrons around the boundary (i.e. sawtooth potential in bulk systems). Replacing the position with polarization \mathbf{P} made it possible to consider potential for electric fields in bulk insulators with electric-field-polarized Wannier functions [6], because the MTP tell one that polarization is independent of the boundary, except that arbitrary modules of polarization are dependent. The first DFT calculations using $\mathbf{E} \cdot \mathbf{P}$ were reported in 1998, but large localization regions were required to get converged field-polarized Wannier functions [7]. In 2002, practical DFT schemes for $\mathbf{E} \cdot \mathbf{P}$ were proposed [5], and they were implemented within the plane wave method [5] or Car–Parrinello method [8]. They succeeded in calculating electronic structures of III-V or II-VI semiconductors under finite electric fields and dielectric properties such as dielectric constants and the Born effective charges. Such a scheme was also implemented in a projector augmented wave (PAW) framework [9].

For realistic conditions, one often need large scale calculations, and localized orbitals such as the linear combination of atomic orbitals (LCAO) method are appropriate in terms of scalability. Interesting models to consider the electric field effect on vacancies, impurities or interfacial systems sometimes require hundreds or thousands of atoms. The MTP for the LCAO scheme demands a conversion from Bloch orbitals to atomic orbitals [10]. Generally, atomic orbitals don't compose the complete basis set, and therefore the Pulay's correction is required. These requirements make the implementation complicated, which is a difficulty in the LCAO scheme. Indeed, there was no more than a density matrix approach in the LCAO scheme for electric field effects [11]. The LCAO implementation of effective potential for finite electric fields is expected to expand the application range to enable one to consider even large scale or realistic models (e.g. vacancies in the diamond NV center).

In this study, we developed the LCAO implementation of the finite electric field scheme and evaluated electronic structures under uniform electric fields. We calculated the dielectric properties of insulators and semiconductors:

dielectric constants and Born effective charges of III-V and II-VI semiconductors and group IV insulating materials. The calculated dielectric properties coincide with the reported computational values. The LCAO implementation will become a powerful tool to investigate electric field effects on large scale systems.

2. Theory

2.1. LCPAO method and modern theory of electric polarization

The LCPAO (linear combination of pseudo atomic orbitals) method uses basis sets localized at atoms and based on atomic orbitals [10]. The required number of basis is much smaller than that in the plane wave method. The fact enables us to solve eigenvalue problems by direct diagonalization. The electronic contribution to electric polarization is described by means of the Berry phase using the Bloch orbitals. While Bloch orbitals can be expressed easily by plane wave basis sets, in the LCPAO method, using localized basis sets of PAOs, Bloch orbitals are given as

$$\langle \mathbf{r} | \psi_{\mu}^{(\sigma \mathbf{k})} \rangle = \frac{1}{\sqrt{N}} \sum_{n=0}^{N-1} e^{i\mathbf{k} \cdot \mathbf{R}_n} \sum_{i\alpha} c_{i\alpha, \mu}^{(\sigma \mathbf{k})} \langle \mathbf{r} - \boldsymbol{\tau}_i - \mathbf{R}_n | \phi_{i\alpha}^{\mathbf{0}} \rangle, \quad (1)$$

where \mathbf{r} is the position, N is the number of cells considered in calculations, “ i ” is the imaginary unit, \mathbf{k} is a wave number, \mathbf{R}_n is the lattice vector for cell n , $c_{i\alpha, \mu}^{(\sigma \mathbf{k})}$ is a LCPAO coefficient connecting a PAO for orbital α belonging to atom i with a Bloch orbital of spin σ and state μ , $\boldsymbol{\tau}_i$ is the position of atom i , and $\phi_{i\alpha}^{\mathbf{R}}$ is a PAO for orbital α belonging to atom i in a cell moved by \mathbf{R} from the original cell. For the LCPAO methods with the Hamiltonian $H_{i\alpha, j\beta}^{(\sigma \mathbf{k})} = \sum_{n=0}^{N-1} e^{i\mathbf{k} \cdot \mathbf{R}_n} \langle \phi_{i\alpha}^{\mathbf{0}} | H_{\sigma} | \phi_{j\beta}^{\mathbf{R}_n} \rangle$ and the overlap matrix $S_{i\alpha, j\beta}^{(\mathbf{k})} = \sum_{n=0}^{N-1} e^{i\mathbf{k} \cdot \mathbf{R}_n} \langle \phi_{i\alpha}^{\mathbf{0}} | \phi_{j\beta}^{\mathbf{R}_n} \rangle$, the Kohn–Sham equation is given as

$$H^{(\sigma \mathbf{k})} c^{(\sigma \mathbf{k})} = \epsilon^{(\sigma \mathbf{k})} S^{(\mathbf{k})} c^{(\sigma \mathbf{k})}, \quad (2)$$

and can be solved by direct diagonalization to get eigenvalues of energies $\epsilon^{(\sigma \mathbf{k})}$. According to the MTP [4], the electronic contribution to electric polarization \mathbf{P}_e in an insulating system with periodic cells is obtained from $\mathbf{G}_a \cdot \mathbf{P}_e$, $\mathbf{G}_b \cdot \mathbf{P}_e$ and $\mathbf{G}_c \cdot \mathbf{P}_e$, which are easy to express by the Berry phase, as

$$\mathbf{G}_a \cdot \mathbf{P}_e = -\frac{ef}{\Omega N_b N_c} \sum_{\sigma} \sum_{I_b=0}^{N_b-1} \sum_{I_c=0}^{N_c-1} \text{Im} \ln \det \prod_{I_a=0}^{N_a-1} M_a^{(\sigma, I_a, I_b, I_c)}, \quad (3)$$

where f is a weighting coefficient of the spin degeneracy per state, \mathbf{G}_a , \mathbf{G}_b and \mathbf{G}_c are the reciprocal lattice vectors for the cell vectors \mathbf{v}_a , \mathbf{v}_b , and \mathbf{v}_c , respectively, e is the elementary charge, Ω is the cell volume, N_a , N_b and N_c are the numbers of k-points to discretize the first Brillouin zone along \mathbf{G}_a , \mathbf{G}_b and \mathbf{G}_c , respectively, $M_{a\mu\nu}^{(\sigma, I_a, I_b, I_c)} = \langle u_{\mu}^{(\sigma\mathbf{k}(I_a, I_b, I_c))} | u_{\nu}^{(\sigma\mathbf{k}(I_a+1, I_b, I_c))} \rangle$ is an overlap matrix of the periodic parts $u_{\mu}^{\sigma\mathbf{k}}$ of occupied Bloch orbitals between adjacent k-points, and $\mathbf{k}(I_a, I_b, I_c) = (I_a/N_a)\mathbf{G}_a + (I_b/N_b)\mathbf{G}_b + (I_c/N_c)\mathbf{G}_c$. The way to express electric polarization by the Berry phase has been successful since it supplies evaluations based on well-defined quantities, instead of direct evaluation of the position \mathbf{r} . $M_{a\mu\nu}^{(\sigma, I_a, I_b, I_c)}$ can be calculated by

$$M_{a\mu\nu}^{(\sigma, I_a, I_b, I_c)} = \left(c^{(\sigma\mathbf{k}(I_a, I_b, I_c))\dagger} T_a^{(\mathbf{k}(I_a+1, I_b, I_c))} c^{(\sigma\mathbf{k}(I_a+1, I_b, I_c))} \right)_{\mu\nu}, \quad (4)$$

where we introduced $T_{ai\alpha, j\beta}^{(\mathbf{k})} = \sum_{n=0}^{N-1} e^{i\mathbf{k}\cdot\mathbf{R}_n} \langle \phi_{i\alpha}^{\mathbf{0}} | e^{-i\frac{\mathbf{G}_a}{N_a}\cdot\mathbf{r}} | \phi_{j\beta}^{\mathbf{R}_n} \rangle$, and μ and ν run over occupied states. Although $M^{(\sigma, \mathbf{k}(I_a, I_b, I_c), \mathbf{k}(I_a+1, I_b, I_c))}$ itself is gauge-dependent, the dependence vanishes by taking the sum over the first Brillouin zone, and electric polarization P_e is evaluated. By introducing $T_{ai\alpha, j\beta}^{(\mathbf{k})}$, the known LCPAO formalism of the MTP [10] becomes a matrix form of Eq. 4 that is the most suitable for computation in terms of the efficiency and simplicity, especially iterative calculations such as self-consistent field (SCF) calculations, because it is enough to prepare $T_{ai\alpha, j\beta}^{(\mathbf{k})}$ once at the beginning of each SCF loop.

2.2. Effective potential for finite electric fields

We start with an expression of electric enthalpy functional \mathcal{F} that is total energy for an insulating system under a finite electric field: $\mathcal{F}[\mathbf{E}] = \mathcal{E}_{\text{KS}} - \Omega \mathbf{E} \cdot \mathbf{P}$ [6], where \mathbf{E} is the electric field, \mathcal{E}_{KS} is the ordinary counterpart of Kohn–Sham total energy described by field-polarized orbitals, and the polarization \mathbf{P} consists of the ionic and electronic contributions: $\mathbf{P} = \mathbf{P}_I + \mathbf{P}_e$. The solution to minimize $\mathcal{F}[\mathbf{E}]$ is desirable so that we can use diagonalization to get solutions for insulators under electric fields in the same way as variational approaches to the ordinary Kohn–Sham equation, for which some treatments for an additional term of effective potential $V = -\Omega \mathbf{E} \cdot \mathbf{P}$ are required. While in the plane wave method, Souza *et al.* suggested the conjugate-gradient method using a gradient $\delta\mathcal{F}/\delta \langle u_{\mu}^{(\sigma\mathbf{k})} |$ [5], for the LCPAO method, we propose doing direct diagonalization by adding matrix elements of the effective potential into the ordinal terms for the Kohn–Sham Hamiltonian H_{σ} . We can extract the

matrix elements of A from a relation of $V = \sum_{\sigma\mathbf{k}} \text{tr}(c^{(\sigma\mathbf{k})\dagger} A^{(\sigma\mathbf{k})} c^{(\sigma\mathbf{k})})$. Taking the derivative of V with respect to the LCPAO coefficients, we get

$$\frac{\partial V}{\partial c_{i\alpha,\mu}^{(\sigma\mathbf{k})*}} = (A^{(\sigma\mathbf{k})} c^{(\sigma\mathbf{k})})_{i\alpha,\mu}. \quad (5)$$

And we expand Eq. 5 with the cell vectors \mathbf{v}_a , \mathbf{v}_b , and \mathbf{v}_c and also get

$$\frac{\partial V}{\partial c_{i\alpha,\mu}^{(\sigma\mathbf{k})*}} = -\Omega \mathbf{E} \cdot \frac{\partial \mathbf{P}}{\partial c_{i\alpha,\mu}^{(\sigma\mathbf{k})*}} = -\Omega \mathbf{E} \cdot \frac{\partial \mathbf{P}_e}{\partial c_{i\alpha,\mu}^{(\sigma\mathbf{k})*}} = -\frac{\Omega}{2\pi} \sum_{\lambda=a,b,c} (\mathbf{E} \cdot \mathbf{v}_\lambda) \frac{\partial}{\partial c_{i\alpha,\mu}^{(\sigma\mathbf{k})*}} (\mathbf{G}_\lambda \cdot \mathbf{P}_e). \quad (6)$$

Here,

$$\frac{\partial}{\partial c_{i\alpha,\mu}^{(\sigma\mathbf{k})*}} (\mathbf{G}_a \cdot \mathbf{P}_e) = -\frac{ef}{\Omega} \left(\left(\frac{O_a^{(\sigma\mathbf{k})} - O_a^{(\sigma\mathbf{k})\dagger}}{2i} \right) c^{(\sigma\mathbf{k})} \right)_{i\alpha,\mu}, \quad (7)$$

where $O_a^{(\sigma\mathbf{k}(I_a, I_b, I_c))} =$

$$\frac{1}{N_b N_c} \mathbf{T}_a^{\mathbf{k}(I_a+1, I_b, I_c)} c^{(\sigma\mathbf{k}(I_a+1, I_b, I_c))} \left(M_a^{(\sigma, I_a, I_b, I_c)} \right)^{-1} \left(M_a^{(\sigma, I_a-1, I_b, I_c)} \right)^{-1} c^{(\sigma\mathbf{k}(I_a-1, I_b, I_c))\dagger} \mathbf{T}_a^{\mathbf{k}(I_a, I_b, I_c)}. \quad (8)$$

Then, we get

$$\frac{\partial V}{\partial c_{i\alpha,\mu}^{(\sigma\mathbf{k})*}} = \left(\left(\frac{ef}{2\pi} \sum_{\lambda=a,b,c} (\mathbf{E} \cdot \mathbf{v}_\lambda) \frac{O_\lambda^{(\sigma\mathbf{k})} - O_\lambda^{(\sigma\mathbf{k})\dagger}}{2i} \right) c^{(\sigma\mathbf{k})} \right)_{i\alpha,\mu}, \quad (9)$$

Therefore, the matrix elements of A is given as

$$A_{i\alpha, j\beta}^{(\sigma\mathbf{k})} = \left(\frac{ef}{2\pi} \sum_{\lambda=a,b,c} (\mathbf{E} \cdot \mathbf{v}_\lambda) \frac{O_\lambda^{(\sigma\mathbf{k})} - O_\lambda^{(\sigma\mathbf{k})\dagger}}{2i} \right)_{i\alpha, j\beta}. \quad (10)$$

In addition, this formalism is compatible with non-collinear spin density functionals and is applicable to cases taking the spin-orbit interaction (SOI) into account.

2.3. Forces under finite electric fields

For forces on atoms induced by the effective potential, the ionic contribution is just $\Omega \mathbf{E} \cdot \frac{\partial P_i}{\partial \mathbf{r}_i} = Z_i e \mathbf{E}$, where Z_i is the core charge of atom i , and the electronic contribution, in the case of the complete basis set, is taken into account without additional terms owing to the Hellmann–Feynman theorem.

In the LCAO representation, the additional terms, that is, Pulay forces are necessary, and they can be given by the derivative of the effective potential through wave functions. The electronic contribution is

$$\Omega \mathbf{E} \cdot \frac{\partial \mathbf{P}_e}{\partial \boldsymbol{\tau}_i} = \frac{ef}{2\pi} \sum_{\lambda=a,b,c} (\mathbf{E} \cdot \mathbf{v}_\lambda) \text{Imtr} \left(\left(\frac{\partial c^\dagger}{\partial \boldsymbol{\tau}_i} \mathbb{T} c + c^\dagger \frac{\partial \mathbb{T}}{\partial \boldsymbol{\tau}_i} c + c^\dagger \mathbb{T} \frac{\partial c}{\partial \boldsymbol{\tau}_i} \right) M^{-1} \right), \quad (11)$$

where $c^\dagger = c^{(\sigma \mathbf{k}(I_a, I_b, I_c))^\dagger}$, $\mathbb{T} = \mathbb{T}_a^{(\mathbf{k}(I_a+1, I_b, I_c))}$, $c = c^{(\sigma \mathbf{k}(I_a+1, I_b, I_c))}$, $M = c^\dagger \mathbb{T} c$, and the trace also sum up the terms with respect to \mathbf{k} . The terms of $\frac{\partial c^\dagger}{\partial \boldsymbol{\tau}_i} \mathbb{T} c + c^\dagger \mathbb{T} \frac{\partial c}{\partial \boldsymbol{\tau}_i}$ are calculated from the energy density matrix $\varepsilon_{i\alpha, j\beta}^{(\sigma \mathbf{R}_n)} = \frac{\Omega}{2\pi} \sum_{\mu}^{\text{occ.}} \sum_{\mathbf{k}} e^{i\mathbf{k} \cdot \mathbf{R}_n} \epsilon_{\mu}^{(\sigma \mathbf{k})} c_{i\alpha, \mu}^{(\sigma \mathbf{k})*} c_{j\beta, \nu}^{(\sigma \mathbf{k})}$ and the derivative of the overlap matrix $s_{i\alpha, j\beta} = \langle \phi_{i\alpha}^0 | \phi_{j\beta}^{\mathbf{R}_n} \rangle$ through a usual way [10]. Therefore, it is only the $c^\dagger \frac{\partial \mathbb{T}}{\partial \boldsymbol{\tau}_i} c$ that need calculating directly.

3. Computational details

We implemented the electric field code based on our LCPAO formalism to the OpenMX code [12–14] (<http://www.openmx-square.org>), which perform first-principles calculations based on the DFT within the local density approximation (LDA) [15] or generalized gradient approximation (GGA) [16]. The norm-conserving pseudopotentials we used included the 2s and 2p electrons for C and O as valence electrons, while the 2p and 3s for Mg; the 3s and 3p for Al, Si, P and S; the 3d and 4s for Zn; the 3d, 4s and 4p for Ga, Ge and As; the 4s and 4p for Se; the 4d and 5s for Cd; the 4d, 5s and 5p for In and Sb. We used a $32 \times 32 \times 32$ regular k-point grid and real space grids corresponding to energy cutoffs larger than 300 Ry to get the converged results of dielectric properties of dielectric constants and Born effective charges. We also used the following *standard* and *precise* PAO basis sets of $Xr\text{-}s n_s p n_p d n_d f n_f$, where X , r and n_s , n_p , n_d and n_f stand for the element, cutoff radius in the unit of Bohr and numbers of s-, p-, d- and f-orbital sets, respectively: for the *standard* one, C6.0-s2p2d1, O6.0-s2p2d1, Mg9.0-s3p2d1, Al7.0-s2p2d1, Si7.0-s2p2d1, P7.0-s2p2d1f1, S7.0-s2p2d1f1, Zn6.0S-s3p2d1, Ga7.0-s3p2d2, Ge7.0-s3p2d2, As7.0-s3p2d2, Se7.0-s3p2d2, Cd7.0-s3p2d2, In7.0-s3p2d2 and Sb7.0-s3p2d2; for the *precise* one, C6.0-s3p2d2, O6.0-s3p2d2, Mg9.0-s3p2d2, Al7.0-s3p2d2, Si7.0-s3p3d2, P7.0-s3p2d2f1, S7.0-s3p2d2f1, Zn6.0S-s3p2d2f1, Ga7.0-s3p2d2f1, Ge7.0-s3p2d2f1, As7.0-s3p2d2f1, Se7.0-s3p2d2f1, Cd7.0-s3p2d2f1, In7.0-s3p2d2f1 and Sb7.0-s3p2d2f1.

For computational models, we used models whose unit cell is the primitive cell of face centered cubic or zinc-blende structures with 2 atoms for computation and applied an electric field of 0.1 GV/m along the a-axis of the conventional cubic cell including 8 atoms. We optimized the lattice constants with the *precise* PAOs and under the LDA, and we neglected their changes due to an external electric field. The optimized lattice constants were $a = 2.4989 \text{ \AA}$ for C, $a = 3.8219 \text{ \AA}$ for Si, $a = 3.8471 \text{ \AA}$ for AlP, $a = 3.9845 \text{ \AA}$ for AlAs, $a = 3.8367 \text{ \AA}$ for GaP, $a = 3.9998 \text{ \AA}$ for GaAs, $a = 4.3184 \text{ \AA}$ for AlSb, $a = 4.1413 \text{ \AA}$ for InP, $a = 3.7529 \text{ \AA}$ for ZnS, $a = 3.9356 \text{ \AA}$ for ZnSe, $a = 4.2526 \text{ \AA}$ for ZnTe, $a = 4.2446 \text{ \AA}$ for CdSe, $a = 4.5433 \text{ \AA}$ for CdTe and $a = 2.9410 \text{ \AA}$ for MgO. The dielectric constant tensor ε were evaluated from

$$\varepsilon_{\alpha\beta} = \delta_{\alpha\beta} + \frac{1}{\epsilon_0} \frac{\partial P_\alpha}{\partial E_\beta} \quad (\alpha, \beta = x, y, z), \quad (12)$$

where the ϵ_0 and $\delta_{\alpha\beta}$ are the electric constant and Kronecker delta, respectively. When the electric polarization induced by the electric field $\Delta\mathbf{P}$ is given without and with atomic relaxation, the $\varepsilon_{\alpha\beta}$ is equal to electronic and static dielectric constants $\varepsilon_{\infty\alpha\beta}$, $\varepsilon_{s\alpha\beta}$, respectively, and we can derive

$$\varepsilon_{\infty\alpha\beta} = 1 + \frac{1}{\epsilon_0} \frac{\Delta P_\alpha}{E_\beta} \Big|_{\delta\tau_i=0}, \quad \varepsilon_{s\alpha\beta} = 1 + \frac{1}{\epsilon_0} \frac{\Delta P_\alpha}{E_\beta} \Big|_{\mathbf{F}=0} \quad (\alpha, \beta = x, y, z), \quad (13)$$

where $\Delta P_\alpha = P_\alpha(\mathbf{E} = E_\beta \hat{\mathbf{e}}_\beta) - P_\alpha(\mathbf{E} = \mathbf{0})$. In addition, through the forces \mathbf{F} on atoms without the atomic relaxation, the Born effective charge tensor Z^* of an atom were also evaluated from

$$Z_{\alpha\beta}^* = \frac{\partial F_\alpha}{\partial E_\beta} \Big|_{\delta\tau_i=0} = \frac{F_\alpha(\mathbf{E} = E_\beta \hat{\mathbf{e}}_\beta) - F_\alpha(\mathbf{E} = \mathbf{0})}{E_\beta} \Big|_{\delta\tau_i=0} \quad (\alpha, \beta = x, y, z). \quad (14)$$

We evaluated the $\varepsilon_{\infty\alpha\beta}$, $\varepsilon_{s\alpha\beta}$ and $Z_{\alpha\beta}^*$, hereinafter the ε_∞ , ε_s and Z^* . The finite electric field was considered after the SCF convergence under the zero field every SCF loop, that is, its effective potential was added after the first SCF convergence. The matrix elements of the effective potential was calculated from the Hamiltonian matrix in the previous SCF iteration and the Overlap matrices. The overlap matrices were prepared in the beginning of each SCF loop. We judged the forces converged when the magnitude of the forces is less than 1×10^{-5} Hartree/Bohr because the Z^* of 1 gives the force of about 2×10^{-4} Hartree/Bohr under the electric field of 0.1 GV/m, and highly precise

evaluation of the forces is essential to description of electronic structures under electric fields and estimation of ϵ_s and Z^* . In the LCPAO method, there is the so-called egg box effect that numerical errors arose from the real space grid, and it is critical in evaluating the forces, dipole moment and stress tensor. The egg box effect can be resolved by the grid cell sampling to repeat evaluation of such quantities several times with the grid shifted and with the density matrix for the LCPAO frozen [10]. The density gradient in the GGA is sensitive to the egg box effect, especially, since it is estimated from the electronic density on the real space grid. Therefore, we applied the grid cell sampling to evaluate the forces precisely by introducing the fine real space grid of at least $100 \times 100 \times 100$ after the SCF convergence in the GGA cases. Another workaround is to consider a stronger electric field to enhance contributions from the electric field to the forces, but it sometimes violates the limitation of the electric field strength due to the Zener breakdown [5], and we didn't treat it in this work. To evaluate the ϵ_s , one need to consider the atomic relaxation. However, the computational cost of the grid cell sampling with such fine grid was too high to continue the relaxation because at least eight evaluations are required (e.g. $2 \times 2 \times 2$ grid shifts). Therefore, we used the "one-shot" grid cell sampling, that is, the forces based on the fine grid were evaluated from the density matrix obtained from the rough grid without the grid shifts.

4. Results and discussion

To validate our formalism, we calculated electronic dielectric constants ϵ_∞ of III-V, II-VI semiconductors and group IV insulators. First, we calculated ϵ_∞ with the LDA to compare our values to those from the plane wave formalism based on the MTP by Souza *et al.* [5]. Our calculated values are shown in Table 1. Our values of the AIP and AIs based on the *precise* PAO basis set coincide with their values, while the ones of the GaP and GaAs has more than 10% and 20% errors. Although our LCPAO formalism is equivalent to Souza *et al.*'s formalism, this mismatch might come from some different conditions such as pseudopotentials. Indeed, our all values are a good agreement with values that recent calculations evaluated under the GGA based on the density functional perturbation theory (DFPT). Next, we calculated ϵ_∞ under the GGA, and the values were improved (i.e. closer to experimental values) for all the systems compared to the LDA. They were a good agreement with values reported in prior works. We confirmed that a moderately large number of

Table 1: Electronic dielectric constants of semiconducting materials. Theoretical values of Ref. [17] were obtained from the DFPT with the GGA, while values of Ref. [5] and Ref. [9] were calculated from the DFT with the LDA and the GGA, respectively, and the finite electric field methods based on the MTP. Our calculated values under three kinds of conditions for the exchange correlation functional and the quality of PAOs are shown.

| System | LDA; <i>standard</i> | LDA; <i>precise</i> | GGA; <i>precise</i> | Ref. (theor.) | Ref. (expt.) |
|--------|----------------------|---------------------|---------------------|-----------------------------|--------------|
| C | 5.61 | 5.67 | 5.67 | 5.9 [17] | 5.7 [18] |
| Si | 12.17 | 12.74 | 12.36 | 12.9 [17] | 11.6 [18] |
| AlP | 8.05 | 8.16 | 7.89 | 8.1 [5,17], 7.84 [9] | 7.4 [18] |
| AlAs | 8.84 | 9.05 | 8.85 | 9.6 [5], 8.80 [9], 9.3 [17] | 8.16 [18] |
| GaP | 10.33 | 10.45 | 9.94 | 9.4 [5], 10.4 [17] | 8.8 [18] |
| GaAs | 13.84 | 14.42 | 13.16 | 11.9 [5], 13.7 [17] | 10.86 [18] |
| AlSb | 10.84 | 11.14 | 10.90 | 11.45 [9], 11.5 [17] | 9.88 [18] |
| InP | 11.07 | 10.91 | 10.08 | 11 [17] | 9.9 [18] |
| ZnS | 5.93 | 6.12 | 5.77 | 5.9 [17] | 5.1 [18] |
| ZnSe | 7.15 | 7.41 | 6.90 | 7.2 [17] | 5.9 [18] |
| ZnTe | 8.35 | 8.86 | 8.24 | 8.9 [17] | 6.9 [18] |
| CdSe | 7.64 | 8.21 | 7.21 | 7.6 [17] | 6.2 [18] |
| CdTe | 8.09 | 8.75 | 7.89 | 8.6 [17] | 7.1 [18] |
| MgO | 3.09 | 3.18 | 3.14 | 3.1 [17] | 3.1 [18] |

k-points are necessary to get the converged values as Souza et al. reported [5]. We also investigated the PAO quality dependence, and the values for the *standard* basis sets are smaller than those for the *precise* ones except the InP. The *standard* basis sets supplies PAOs around atom centers in a more narrow domain than the *precise* basis sets. More localized description of electronic states through the *standard* basis sets can confine the electronic distribution more strongly and suppress the ε_∞ . These results demonstrated that our LCPAO implementation of effective potential for the finite electric field was correct.

To investigate influence of the SOI, we focused on ZnTe and CdTe including the tellurium that is the heaviest element in our systems. In the case that we considered the SOI with the *precise* basis set under the GGA, the ε_∞ of ZnTe and CdTe became 8.37 and 8.10 and increased by 0.13 and 0.21, respectively. The strong SOI can drastically change the electronic structure so that these increases occur. In fact, the band gap of ZnTe and CdTe changed from and 1.73 eV and 1.04 eV to and 1.60 eV and 0.77 eV after including the SOI, respectively; see also Appendix A about the relation between the band gap and ε_∞ . The ε_∞ of AlSb also increased by 0.11, and it became 11.01. Our results illustrated that for systems including heavy-element atoms, the SOI effect on the ε_∞ should be considered, and the implementation for the SOI is important.

As shown in Table 2, we also calculated the Born effective charges Z^* of cations except for the group IV systems to validate our formalism of forces on atoms under the electric fields. Our calculated results were robust with respect to exchange correlation functionals, and each Z^* under the LDA is almost equal to that under the GGA. Our values were a good agreement with not only the theoretical values but also experimental values in the previous studies, and the mean absolute error (MAE) of Z^* between our values and the experimental values with respect to the systems was $\sim 6\%$. We concluded, therefore, that our formalism of forces under the finite electric fields was also correct. In including the SOI, however, only negligible changes appeared. Although a fine real space grid allowed us to get converged values, we confirmed that even a rough real space grid could provide good values, which suggests that the computational cost can be reduced in calculating only the Z^* .

Then, we evaluated the atomic relaxation under finite electric fields through the static dielectric constants ε_s . As shown in Table 3, the values based on the LDA and the GGA were successfully reproduced except GaAs. The LDA value

Table 2: Born effective charges of semiconducting materials. Theoretical values of Refs. [19–21] were obtained from the DFT with the LDA and the finite difference method based on the MTP, while those of Refs. [5,8] and Ref. [9] were calculated from the DFT with the LDA and the GGA, respectively, and the finite electric field methods based on the MTP. Our calculated values under two kinds of conditions for the exchange correlation functional and the quality of PAOs are shown. The value of Ref. [21] is that of the anion.

| System | LDA; <i>precise</i> | GGA; <i>precise</i> | Ref. (theor.) | Ref. (expt.) |
|--------|---------------------|---------------------|---|--------------|
| AIP | 2.19 | 2.20 | 2.24 [5], 2.23 [9], 2.20 [19] | 2.15 [22] |
| AlAs | 2.12 | 2.09 | 2.14 [5], 2.110 [20], 2.17 [9], 2.12 [19] | 2.20 [23] |
| GaP | 2.05 | 2.11 | 2.10 [5], 2.06 [19] | 2.16 [24] |
| GaAs | 2.09 | 2.10 | 2.00 [5], 2.18 [20], 2.08 [19] | 2.18 [23] |
| AlSb | 1.81 | 1.75 | 1.83 [9], 1.81 [19] | 1.93 [25] |
| InP | 2.44 | 2.48 | 2.50 [19] | 2.55 [26] |
| ZnS | 1.87 | 1.89 | -1.99 [21] | 2.15 [26] |
| ZnSe | 1.95 | 1.95 | 2.12 [27] | 2.03 [26] |
| ZnTe | 1.87 | 1.86 | | 2.00 [26] |
| CdSe | 2.19 | 2.17 | | 2.25 [26] |
| CdTe | 2.09 | 2.08 | | 2.35 [26] |
| MgO | 1.98 | 1.98 | 1.96 [8] | 1.77 [26] |

Table 3: Static dielectric constants of semiconducting materials. Theoretical values of Ref. [5,8] and Ref. [9] were calculated from the DFT with the LDA and the GGA, respectively, and the finite electric field methods based on the MTP. Our calculated values under two kinds of conditions for the exchange correlation functional and the quality of PAOs are shown.

| System | LDA; <i>precise</i> | GGA; <i>precise</i> | Ref. (theor.) | Ref. (expt.) |
|--------|---------------------|---------------------|---------------------|--------------|
| AIP | 10.26 | 9.94 | 10.2 [5], 10.26 [9] | 9.6 [18] |
| AlAs | 10.90 | 10.56 | 11.5 [5], 11.05 [9] | 10.6 [18] |
| GaP | 11.96 | 11.69 | 11.2 [5] | 11.0 [18] |
| GaAs | 19.28 | 14.38 | 13.5 [5] | 12.90 [18] |
| MgO | 7.92 | 8.79 | 7.93 [8] | 9.8 [18] |

of GaAs was overestimated compared to the results of previous studies because our calculated band gap of 0.25 eV was rather underestimated compared to an experimental value of 1.579 eV [28], which made more delocalized pictures of electrons to give the overestimation. The GGA values were closer to the experimental ones than the LDA, and the AlP, AlAs and GaP values had errors within 7%, while even errors the GaAs and MgO values were within $\sim 30\%$. Although we reproduced the LDA value of MgO reported in the previous theoretical study [8], there was the mismatch of the MgO values between the experimental and theoretical ones. With an experimental lattice constant of 4.212Å [29] for its conventional cell, the ϵ_s of MgO became 9.56, that is, it approaches the experimental ϵ_∞ of 9.8 [18], although our lattice constant is 1% smaller compared to the experimental one. In the atomic relaxation, the precision of the forces on atoms is most important, and even minor errors with the magnitude of 10^{-4} Hartree/Bohr can reflect large errors of the ϵ_s . As a result, it suggests that not only a fine k-space grid but also a fine real space grid is required to describe the movements of atoms in solids under a finite electric field. Although the computational cost of the ordinary grid cell sampling with a fine real space grid was too high to continue the relaxation, we confirmed that the “one shot” grid cell sampling was efficient and effective to avoid the numerical errors induced by the real space grid or density gradient. Finally, it was proved that our formalism for the forces was correct, and that it can be applied to not only atomic relaxation but also molecular dynamics under finite electric fields.

5. Conclusion

We developed the LCPAO scheme of a finite electric field method based on the MTP, and investigated the PAO dependence and exchange correlation dependence by performing systematic calculations. Our implementation successfully reproduced the electronic and static dielectric constants and Born effective charges of III-V and II-VI semiconductors and group IV insulating materials. We confirmed that the implementation for the SOI is necessary for systems including heavy elements. Our LCPAO implementation is expected to have more advantages compared to the conventional formalism such as the plane wave method in terms of not only efficiency but also extensibility: large scale calculations modeling realistic systems through the $O(N)$ method, and the atomic or orbital decomposition of the effective potential, for example. Our formalism will expand the problem size so that even complicated systems such

as devices are easier to consider, and the molecular dynamics of complicated systems such as batteries under a finite electric field can be applied with a lower computational cost.

Acknowledgement

This work was supported by JSPS KAKENHI Grants Numbers JP18J21257, JP18H04481, JP19H02554, JP20K15115. The computation in this work has been done using the facilities of the Supercomputer Center, the Institute for Solid State Physics, the University of Tokyo. The computation was carried out using the computer resource offered under the category of General Projects by Research Institute for Information Technology, Kyushu University. This work used computational resources of the supercomputer Fugaku provided by the RIKEN Center for Computational Science through the HPCI System Research Project (Project ID: hp210305).

Appendix A: Correlation between the ε_∞ and the band gap

Figure 1 shows that there was a trade-off between the calculated ε_∞ and band gap. This trend coincides with a picture that the electron distribution is more localized for the wider band gap.

References

- [1] H. Ehrenreich and M. H. Cohen, *Phys. Rev.* **115**, 786 (1959).
- [2] L. J. Sham, *Phys. Rev.* **188**, 1431 (1969).
- [3] R. M. Pick, M. H. Cohen, and R. M. Martin, *Phys. Rev. B* **1**, 910 (1970).
- [4] R. D. King-Smith and D. Vanderbilt, *Phys. Rev. B* **47**, 1651 (1993).
- [5] I. Souza, J. Íñiguez, and D. Vanderbilt, *Phys. Rev. Lett.* **89**, 9 (2002).
- [6] R. W. Nunes and D. Vanderbilt, *Phys. Rev. Lett.* **73**, 712 (1994).
- [7] P. Fernández, A. Dal Corso, and A. Baldereschi, *Phys. Rev. B - Condens. Matter Mater. Phys.* **58**, R7480 (1998).

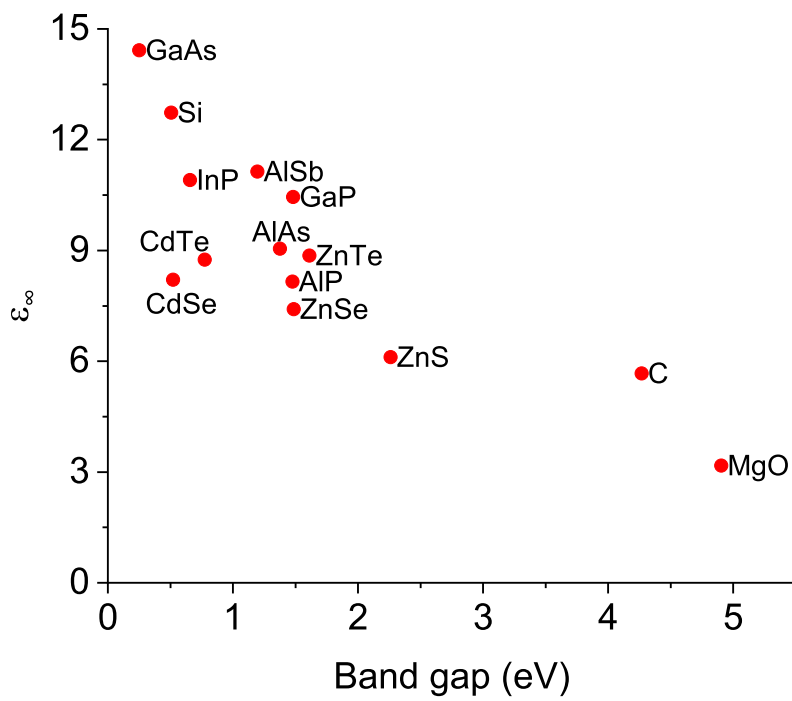


Figure 1: The ϵ_{∞} versus the band gap. These are calculated with the LDA functional and *precise* basis sets.

- [8] P. Umari and A. Pasquarello, Phys. Rev. Lett. **89**, 1 (2002).
- [9] J. W. Zwanziger, J. Galbraith, Y. Kipouros, M. Torrent, M. Giantomassi, and X. Gonze, Comput. Mater. Sci. **58**, 113 (2012).
- [10] J. M. Soler, E. Artacho, J. D. Gale, A. García, J. Junquera, P. Ordejón, and D. Sánchez-Portal, J. Phys. Condens. Matter **14**, 2745 (2002).
- [11] H. J. Xiang, J. Yang, J. G. Hou, and Q. Zhu, Phys. Rev. Lett. **97**, 1 (2006).
- [12] T. Ozaki, Phys. Rev. B - Condens. Matter Mater. Phys. **67**, 1 (2003).
- [13] T. Ozaki and H. Kino, Phys. Rev. B - Condens. Matter Mater. Phys. **69**, 1 (2004).
- [14] T. Ozaki and H. Kino, Phys. Rev. B - Condens. Matter Mater. Phys. **72**, 1 (2005).
- [15] D. M. Ceperley and B. J. Alder, Phys. Rev. Lett. **45**, 566 (1980).
- [16] J. P. Perdew, K. Burke, and M. Ernzerhof, Phys. Rev. Lett. **77**, 3865 (1996).
- [17] Y. Hinuma, Y. Kumagai, I. Tanaka, and F. Oba, Phys. Rev. B **95**, (2017).
- [18] in *Properties of Group-IV, III-v and II-VI Semiconductors* (John Wiley & Sons, Ltd, 2005), pp. 211–281.
- [19] N. Benyahia, A. Zaoui, D. Madouri, and M. Ferhat, J. Appl. Phys. **121**, (2017).
- [20] X. Wang and D. Vanderbilt, Phys. Rev. B - Condens. Matter Mater. Phys. **75**, 1 (2007).
- [21] A. Dal Corso, M. Posternak, R. Resta, and A. Baldereschi, Phys. Rev. B **50**, 10715 (1994).
- [22] S. Lakel, F. Okbi, M. Ibrir, and K. Almi, AIP Conf. Proc. **1653**, (2015).
- [23] G. S. Spencer, A. C. Ho, J. Menéndez, R. Droopad, H. Fathollahnejad, and G. N. Maracas, Phys. Rev. B **50**, 14125 (1994).
- [24] N. S. Samarasingha and S. Zollner, J. Vac. Sci. Technol. B **39**, 052201 (2021).

- [25] S. Ves, K. Strössner, and M. Cardona, *Solid State Commun.* **57**, 483 (1986).
- [26] G. Lucovsky, R. M. Martin, and E. Burstein, *Phys. Rev. B* **4**, 1367 (1971).
- [27] D. Wang, X. Zhang, B. Li, L. Liu, and D. Z. Shen, *AIP Adv.* **4**, (2014).
- [28] W. M. Haynes, *CRC Handbook of Chemistry and Physics* (CRC Press, 2016).
- [29] D. Sun, H. Enoki, F. Gingl, and E. Akiba, *J. Alloys Compd.* **285**, 279 (1999).